Optical and EPR spectroscopy of Er³⁺ in lithium yttrium borate, Li₆Y(BO₃)₃:Er single crystals

L. Kovács[1], S. Arceiz Casas[2], G. Corradi[1], É. Tichy-Rács[1], L. Kocsor[1], K. Lengyel[1], W. Ryba-Romanowski[3], A. Strzep[3], A. Scholle[2], S. Greulich-Weber[2]

[1] Wigner Research Centre for Physics, Hungarian Academy of Sciences, Budapest, Hungary,

[2]University Paderborn, Germany

[3] Institute of Low Temperature and Structure Research, Polish Academy of Sciences, Wroclaw, Poland

Abstract

The energy levels of Er³⁺ ions have been determined in lithium yttrium borate (Li₆Y(BO₃)₃) single crystals in a wide spectral range between 6000 – 40000 cm⁻¹ together with an analysis of the ground state, using optical and EPR spectroscopy. The crystal field splittings of the $^4I_{15/2}$ ground state and those of nearly all excited states up to the $^4D_{7/2}$ manifold have been obtained at low temperature from luminescence (T = 5 K) and absorption (T = 9 K) measurements, respectively. The numbers of experimentally observed Stark sublevels agree well with those expected theoretically for Er³⁺ ions occupying a single low symmetry (C₁) site. A full set of g-factor and ^{167}Er hyperfine tensor parameters are presented for the ground state characterized by EPR; the measured Orbach-type spin-relaxation rates viz. the involved activation energies correspond to the optically derived lowest excited sublevels.

Keywords: spectroscopy; EPR; borate; rare-earth

1. Introduction

Li₆Y(BO₃)₃ (LYB) single crystals having a monoclinic crystal structure belonging to the P2₁/c space group [1] are good candidates for laser materials due to their flexibility and the easy incorporation of the rare earth (RE) dopants (e.g. Nd³⁺, Eu³⁺, Er³⁺, Yb³⁺) [2, 3]. Er³⁺ ions are especially interesting for their near infrared emission suitable for optical telecommunication systems. Diode-pumped 1594 nm laser performance has already been realized in Er and Yb co-doped LYB [4]. The region near 1000 nm is also interesting for laser operation [5]. The transitions $^2F_{5/2} - ^2F_{7/2}$ and $^4I_{11/2} - ^4I_{15/2}$ of Yb³⁺ and Er³⁺ ions, respectively, occurring in the wavelength range of 960-980 nm are promising candidates for coherent quantum optical applications. LYB single crystals may serve as excellent host matrices with long enough dipole relaxation times of the RE ions suitable for quantum optical experiments where atomic coherence plays a crucial role [6]. In addition, RE doped single crystals and polycrystalline LYB and its gadolinium counterpart LGB are also used as scintillators for thermal neutron

detection and phosphors for white light emission [7, 8]. For most applications the crucial point is the accurate determination of the energy levels of the RE ions in the matrix. The LYB:Yb^{3+} system has been well documented by Sablayrolles et al [3, 5, 9], Jubera et al [10], and Brenier et al [11]. Although some spectroscopic properties of Er^{3+} in LYB measured at room temperature have also been reported [12, 13], a detailed spectroscopic analysis of the LYB:Er^{3+} system is still missing. Recently a preliminary study of the absorption spectra of Er^{3+} ions at 2 K has been published in the narrow 370 – 700 nm visible wavelength range [14]. Our aim is to characterize the energy levels of Er^{3+} in LYB crystals obtained at low temperature in a wide spectral range from the infrared to the ultraviolet by using absorption and luminescence spectroscopies, together with a detailed EPR analysis of the ground state. The site occupation of Er^{3+} and the possible RE pair formation found e.g. in Yb^{3+} doped LYB, which may induce modifications in the Stark component splitting [10], will also be discussed for Er^{3+} doped LYB single crystals.

2. Experimental

LYB single crystals doped either with 0.05 or 1 mol% Er were grown by the Czochralski method as described in detail in ref. [15]. The crystals were oriented by X-ray diffraction and cut to platelets of ~2 mm thickness with their large face perpendicular to the crystallographic *b* axis (the twofold screw axis) and a longer edge oriented along the normal of the (-102) Miller plane. For optical absorption experiments the samples were placed in a closed-cycle helium cryostat and measured between 9 – 300 K by a Bruker IFS 66v/S FTIR spectrometer in the 6000 – 40000 cm^{-1} wavenumber range with a resolution of 0.2 cm^{-1}. Some transitions of the Er^{3+} ions have also been measured at 8 K using a Bruker IFS 120 spectrometer with a resolution of 0.03 cm^{-1}. The luminescence spectra measured using an Optron Dong-Woo Fluorometer System at 5 K were excited by a 488 nm Ar^{+} laser. EPR spectra were taken in the temperature interval between 5 and 80 K in the X-band using a custom-built X-band spectrometer.

3. Results and Discussion

3.1 Absorption spectra

The Er^{3+} ion has 11 electrons in the 4f shell. Since the f orbits are well shielded by the outer 5s and 5p orbits, they are weakly affected by the ligand ions in a crystal. Therefore the $^{2S+1}L_J$ spin-orbit interaction terms are only slightly perturbed by the weak crystalline field, and can be relatively easily identified based on the Dieke diagram [16]. Since LYB is transparent in the UV up to about 180 nm (~55000 cm^{-1}) a long series of transitions from the $^4I_{15/2}$ ground state was detected by absorption spectroscopy. The $^4I_{13/2}$, $^4I_{11/2}$, $^4I_{9/2}$, $^4F_{9/2}$, $^4S_{3/2}$, $^2H_{11/2}$, $^4F_{7/2}$, $^4F_{5/2}$, $^4F_{3/2}$, $^2H_{9/2}$, $^4G_{11/2}$, $^2G_{9/2}$, $^2G_{7/2}$, $^2P_{3/2}$, $^4G_{7/2}$, $^2D_{5/2}$, $^4G_{9/2}$, $^4D_{5/2}$, and $^4D_{7/2}$ excited states were identified in the spectra between 6000 – 40000 cm^{-1} (see Table 1). Figures 1 and 2 each show 3 examples in the infrared and ultraviolet regions, respectively, measured on samples containing 1 mol% Er. The Stark sublevels due to crystal field splittings for Er^{3+} ions are well

resolved in the spectra. Many absorption lines especially in the IR range are as narrow as 0.5 cm^{-1} at T = 9 K allowing the accurate determination of the energy levels. The narrowest absorption lines of about 0.15 cm^{-1}, measured using the high resolution Bruker IFS 120 spectrometer, have been observed for the two lowest energy Stark levels of the $^4I_{13/2}$ transition on samples doped with 0.05 mol% Er. Table 1 summarizes all energy levels of Er^{3+} in the LYB crystal measured at 9 K between 6000 – 40000 cm^{-1}. The $^2H_{9/2}$, $^2G_{9/2}$, and $^4G_{9/2}$ multiplets are often labelled as $^2G_{9/2}$, $^4G_{9/2}$, and $^2H_{9/2}$ [17, 18, 19, 20], respectively, i.e. some authors use a different order for the energy terms. Since the number of crystal field components is five in each multiplet, a unambiguous identification of these terms requires polarization spectroscopy which is outside the scope of this paper. The transitions to the $^2G_{9/2}$ and $^2K_{15/2}$ multiplets show considerable overlap allowing the separation of only eight out of the expected 5+8 Stark components. None of the absorption bands related to the $^2K_{13/2}$, $^2P_{1/2}$, and $^4G_{5/2}$ levels could be detected either, probably due to their weak oscillator strength. The number of Stark sublevels ((2J+1)/2) for all other terms perfectly agrees with that expected theoretically for Er^{3+} ions occupying a single low symmetry (C$_1$) site. The energy values observed in the visible spectral range from $^4F_{9/2}$ to $^4G_{11/2}$ are in perfect agreement with those published recently by Skvortsov et al [14]. The obtained energy levels agree quite well also with those observed for Er^{3+} e.g. in garnets and halides [17-20] and in other borate crystals like yttrium aluminum borate (YAB) [21]. The maximum Stark splittings ΔE of the transitions shown in the last column of Table 1 also agree with those reported in [17-21] and references therein. A detailed analysis of the orientation and polarization dependences of the absorption spectra of Er and other RE ions in monoclinic LYB crystals will be published elsewhere.

At somewhat higher temperatures the absorption spectra show additional lines (for T=80 K see Fig. 3) which can be attributed to the thermal population of higher Stark sublevels of the ground state. As indicated in the figure, most lines seen at 9 K (see bottom part of Fig. 1 and lines numbered 1-7 in Fig. 3) acquire satellites corresponding to transitions from higher Stark levels of the ground state to the same target level. Up to three satellites with fairly coinciding spacings of 46, 77 and 115 cm^{-1} can be observed.

3.2 Luminescence

These and additional Stark sublevels of the $^4I_{15/2}$ ground state can be determined with higher precision by luminescence spectroscopy. Fig. 4 shows the $^4I_{13/2} \rightarrow {}^4I_{15/2}$ luminescence spectrum excited by a 488 nm line of an Argon ion laser at T = 5 K on a LYB crystal with 1 mol% Er. The overall crystal field splitting of the ground state amounts to 524 cm^{-1}. Owing to the high cut-off phonon energy of the host at about 1400 cm^{-1} the multiphonon relaxation governs the decay processes of excited states above the $^4I_{13/2}$, the single luminescent level in this system. The decay curve of the luminescence originating from the $^4I_{13/2}$ level follows a single exponential time dependence with a lifetime of 394 and 378 μs at T = 300 K and T = 5 K, respectively (see Fig. 5), in relatively good agreement with the 0.448 ms value measured at room temperature under excitation at 1480 nm as reported earlier by Zhao [12].

There is general agreement in the literature that trivalent RE dopants occupy the unique Y^{3+} site in LYB single crystals. Surrounding each Y/RE ion there are 8 oxygen atoms forming a distorted tetragonal prism [1]. The resulting YO_8 polyhedra form chains along the *c*-axis sharing edges. The Y-Y intrachain distance is at about 3.85 Å. In heavily Yb-doped single crystals, however, two zero-phonon lines were observed in the transmission and emission spectra indicating the presence of two kinds of non-equivalent Yb^{3+} ions in the lattice [11]. One of them is at the regular Y^{3+} site, while the other was later attributed to members of Yb^{3+} pairs at neighbouring Y^{3+} sites by a detailed luminescence and EPR spectroscopic study in Yb-doped LYB and LGB crystals [10]. The interatomic distance R = 3.856 Å within the Yb^{3+}-Yb^{3+} pairs calculated from the EPR spectra is in good agreement with the above X-ray diffraction value. Neither our absorption nor the luminescence measurements on both 0.05 and 1 mol% Er-doped LYB crystals showed additional Stark component splitting, so we may conclude that Er^{3+} ions essentially occupy only regular Y^{3+} sites in our samples. This may be attributed either to the lower dopant concentration or the lower pair formation ability of Er^{3+} ions.

3.3 EPR

The EPR spectra at low temperatures reproduced for 0.05 mol% Er in Fig. 6, show the presence of a dominant Er^{3+} centre. Two magnetically non-equivalent centre families due to the C_{2h} point symmetry of the crystal are observed. The central line of each group is due to the Er isotopes having zero nuclear spin (^{166}Er and ^{168}Er) while the fully resolved hyperfine structure is due to the ^{167}Er isotope having a I=7/2 nuclear spin and a natural abundance of 22.94%. To describe the spectra an effective ground-state spin S=1/2 and a spin Hamiltonian

$$H = \mu_B \textbf{\textit{BgS}} + \textbf{\textit{SAI}}$$

have been used where μ_B is the Bohr magneton; the Zeeman term contains the external magnetic field vector **B** together with the **g** tensor, and the second term the hyperfine tensor **A** relevant only for ^{167}Er. The line positions were calculated using the *EasySpin* computer code [22].

For a unambiguous assignment of the centre families required for a full determination of the **g** and ^{137}**A** tensors angular dependent spectra had to be measured for magnetic field orientations in four different crystallographic planes (Fig. 7). This is due to the low symmetry of both the crystal host and the paramagnetic centre as described in detail in the literature [23, 24]. The first three panels of Fig. 7 correspond to rotations of **B** in planes defined by the right-handed orthogonal axes system x_E, y_E, z_E, where $z_E \parallel b$, and y_E is along the normal of the planes with Miller indices (-102); accordingly the x_E axis makes angles 26.94° and 78.38° with the *a* and *c* crystallographic axes, respectively. Panel 4 approximately corresponds to a rotation from y_E (denoted $[010]_E$ in the x_E, y_E, z_E system) towards the $[-101]_E$ direction (note compressed field axis). Numbers 1 and 2 refer to magnetically non-equivalent Er centre families, points to experimental data and lines to simulated values using best-fit spin-Hamiltonian parameters given in Table 2. The Euler angles in Table 2 (based on the zyz convention used also in *EasySpin*), transfer the x_E, y_E, z_E axes to the tensor's principal axes. Using only data in the

first three planes but with different centre family labelling yielded also a second "solution" (see [23, 24]) but this lead to grossly deviating line positions for the fourth plane. The data were redundant enough to take into account small misalignments/tilts of the crystal sample in the resonator. The corresponding 3-parameter sets for each plane were determined as additional parameters in the g-tensor fitting procedure carried out simultaneously for the first three planes. These auxiliary parameters turned out to have nearly negligible values for these planes, and have been used, together with the derived g-tensor components, for hyperfine fitting procedures. Sample misorientation was found to be more sizable in the comparison done for fourth-plane experiments where the sample had to be mounted in a diagonal position relative to the sample holder. Accordingly the simulations shown in panel 4 include the corresponding misalignment parameters as well. The data in Table 2 reflect the common origins of the anisotropy of the spin-Hamiltonian tensors g and ^{137}A.

The errors of the best-fit values are only partly due to the residual peak-to-peak linewidth ΔB_o ≈ 0.5 mT measured at 6K in the low field region for the sample with 0.05 mol% Er content. The slightly larger error interval for the first Euler angle is due to the difficulty of reproducing the direction of the x_E and y_E axes not fixed by crystal symmetry. The lines broadened with increasing magnetic field leading to the disappearance of the lines above 350 mT, which explains the large error bar of the smallest principal value for both the g and ^{137}A tensor.

The EPR spectra also showed fast temperature broadening and could not be observed above 25 K. The peak to peak linewidth showed an Arrhenius type

$$\Delta B = \Delta B_o + C \exp(-\Delta E_a/kT)$$

temperature dependence shown for the central lines of two centre families for magnetic fields near 100 mT in Fig. 8. This indicates an Orbach-type spin-lattice relaxation process with the observed activation energy $\Delta E_a = (43 \pm 10)$ cm^{-1} and coupling constant C = (26 ± 8) mT. These parameters showed only weak orientation dependence within the error limits (see the slightly different linewidths shown for the two centre families in Fig. 8 which can also be attributed to the slightly different magnetic fields). The activation energy determined from EPR linewidth data is in good agreement with the energy of the first excited Stark sublevel at (47 ± 1) cm^{-1} derived from the optical data (Figs. 3, 4 and Table 1) proving that spin-lattice relaxation takes place via thermal excitation to this sublevel.

The EPR spectra of the LYB sample containing 1 mol% Er were essentially identical to those measured for lower concentration apart from line broadening characterized by $\Delta B \approx 1.4$ mT at 6K and attributed to interaction between the Er centres. Very weak additional signals possibly due to pair centres have also been detected for some orientations but could not be analyzed in detail.

4. Conclusions

The Er^{3+} centre in LYB has been characterized by optical and EPR spectroscopy. A series of transitions from and to the $^4I_{15/2}$ ground state and their crystal field splittings were measured

using high resolution optical spectroscopy. Since the crystal is highly transparent in the UV range 90 Stark components of 20 manifolds ranging from the $^4I_{15/2}$ ground to the $^4D_{7/2}$ excited multiplet could be identified in the spectra between 6000 – 40000 cm^{-1}. Spin-Hamiltonian and spin-lattice relaxation data have been obtained for the ground state. The number of spectroscopic components and their linewidths both in optical and paramagnetic resonance spectroscopy indicate that the Er^{3+} dopant substitutes at an essentially unperturbed Y site in Li$_6$Y(BO$_3$)$_3$.

Acknowledgements

Table 1. Energy levels (cm^{-1}) of Er^{3+} in LYB observed at T = 9 K by absorption and emission spectroscopies. Number of expected lines and total splitting are indicated for each term.

Energy level		Number of lines	Δ E	Energy level		Number of lines	Δ E
$^4I_{15/2}$	0	8	524	$^2H_{9/2}$[a]	24465	5	352
	47				24597		
	76				24641		
	113				24784		
	368				24817		
	466			$^4G_{11/2}$	26308	6	337
	497				26335		
	524				26387		
$^4I_{13/2}$	6580	7	292		26551		
	6600				26592		
	6633				26645		
	6760			$^2G_{9/2}$[b]$+^2K_{15/2}$	27393	5+8	
	6829				27411		
	6850				27489		
	6872				27516		
$^4I_{11/2}$	10276	6	136		27525		
	10297				27543		
	10358				27582		
	10396				27705		
	10403				…		
	10412			$^2G_{7/2}$	28045	4	133
$^4I_{9/2}$	12338	5	430		28134		
	12534				28152		
	12585				28178		
	12725			$^2P_{3/2}$	31534	2	86
	12768				31620		
$^4F_{9/2}$	15304	5	211	$^2K_{13/2}$	…	7	
	15364			$^2P_{1/2}$	…	1	
	15384			$^4G_{5/2}$	…	3	
	15481			$^4G_{7/2}$	34014	4	197
	15515				34048		
$^4S_{3/2}$	18435	2	58		34095		
	18493				34211		
$^2H_{11/2}$	19150	6	246	$^2D_{5/2}$	34809	3	114
	19178				34857		
	19208				34923		
	19327			$^4G_{9/2}$[c]	36367	5	436
	19349				36423		
	19396				36525		
$^4F_{7/2}$	20555	4	170		36593		
	20595				36803		
	20677			$^4D_{5/2}$	38515	3	46
	20725				38550		
$^4F_{5/2}$	22247	3	78		38561		
	22286			$^4D_{7/2}$	39045	4	361
	22325				39163		
$^4F_{3/2}$	22617	2	65		39252		
	22682				39406		

[a] This multiplet is often labelled as $^2G_{9/2}$ (see e.g. refs. [17-19])

[b] This multiplet is often labelled as $^4G_{9/2}$ (see e.g. refs. [17-19])

[c] This multiplet is often labelled as $^2H_{9/2}$ (see e.g. refs. [17-20])

Table 2 Spin-Hamiltonian parameters for the ground state of the Er^{3+} centre in LYB.

Tensor	Principal values			Euler angles (^{o})		
g	6.25 (±2)	0.67 (±20)	8.00 (±2)	-5.1 (±3.0)	46.0 (±0.2)	37.0 (±0.2)
^{137}A (MHz)	657 (± 3)	300 (±200)	847 (±3)	1.5. (±3.0)	44.4 (±1.0)	40.5 (±1.0)

Figure captions

Figure 1. Absorption spectra of Er^{3+} ions in LYB crystals in the infrared spectral range measured at T = 9 K. Transitions from the $^4I_{15/2}$ ground state to the $^4I_{13/2}$, $^4I_{11/2}$ and $^4I_{9/2}$ multiplets are presented. The number of lines is equal to (2S+1)/2, see text.

Figure 2. Absorption spectra of Er^{3+} ions in LYB crystals in the ultraviolet spectral range measured at T = 9 K. Transitions from the $^4I_{15/2}$ ground state to the $^4G_{11/2}$, $^4G_{9/2}$ and $^4D_{7/2}$ terms are presented.

Figure 3 Absorption spectra at T=80 K for the $^4I_{15/2} \rightarrow ^4I_{13/2}$ transition of LYB:Er^{3+}. Each of the transitions numbered 1-7 seen also at 9K have satellites corresponding to transitions from thermally populated higher Stark sublevels of the ground state to the same target level.

Figure 4. Luminescence spectrum of LYB:Er^{3+} excited by an Ar-ion laser at 488 nm. Arrows indicate the 8 Stark sublevels of the $^4I_{15/2}$ ground state.

Figure 5. Decay of the luminescence intensity of the $^4I_{13/2}$ level of LYB:Er^{3+} measured at T = 300 K and T = 5 K.

Figure 6. EPR spectra of a LYB sample containing 0.05 mol% Er taken at T = 6 K in the X-band for the magnetic field B in the y_E-z_E crystallographic plane for rotation steps of 5° (upper part) and enlarged spectrum for a rotation of ~50° from the y_E axis (lower part).

Figure 7. Angular dependence of EPR line positions in four crystallographic planes (see text and note the compressed field axis for panel 4). Numbers 1 and 2 refer to magnetically non-equivalent Er centre families, points to experimental data, the lines (solid for nonmagnetic isotopes of Er and dashed for hyperfine octets due to ^{167}Er) were simulated using the parameter values given in Table 2, taking into account for panel 4 the misalignment of the crystal.

Figure 8. Temperature dependence of the EPR linewidth for a selected direction of the magnetic field **B**. The derived activation energies for the two centre families are ~45 cm^{-1} and ~40 cm^{-1}, the line shown corresponds to the average slope.
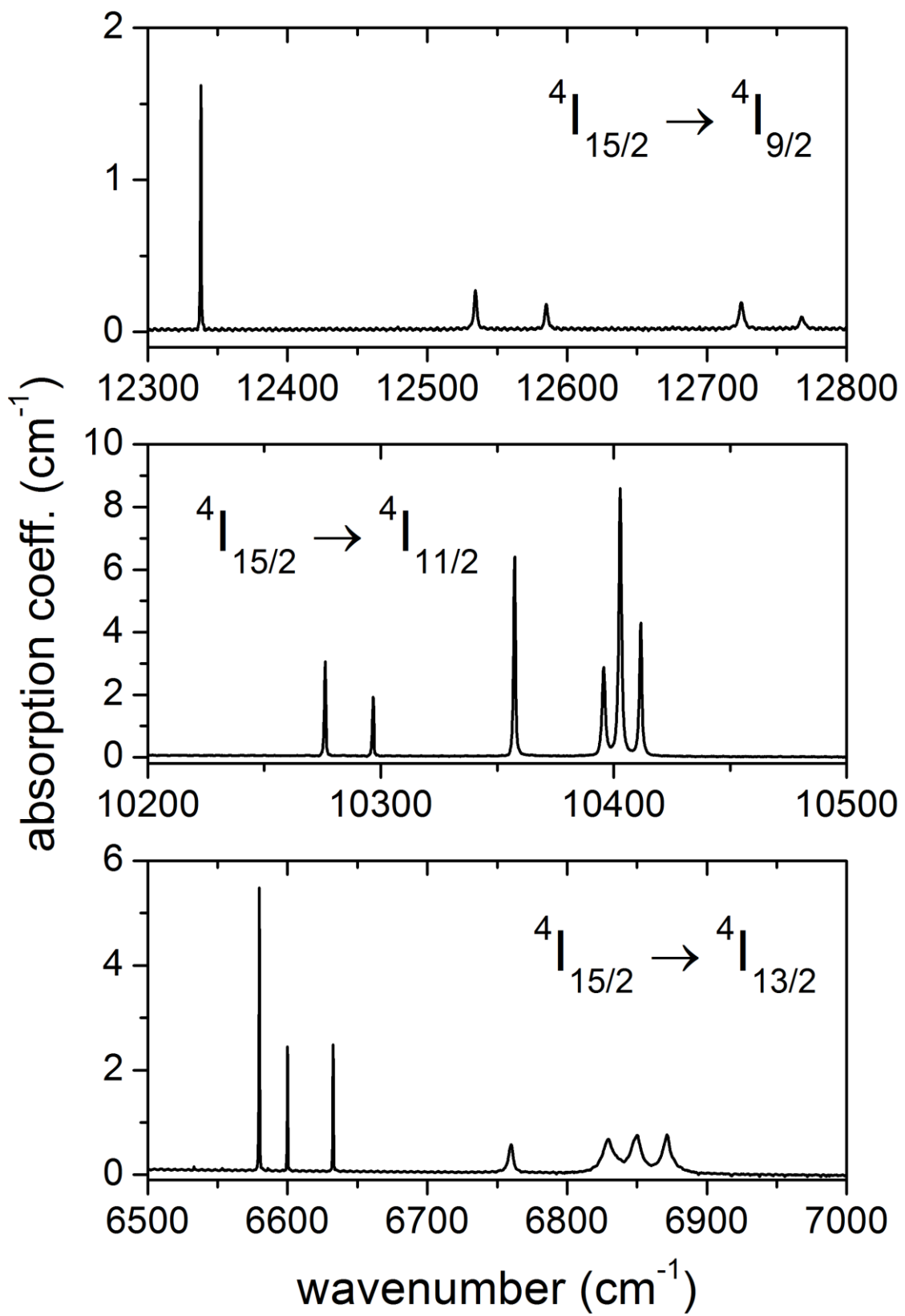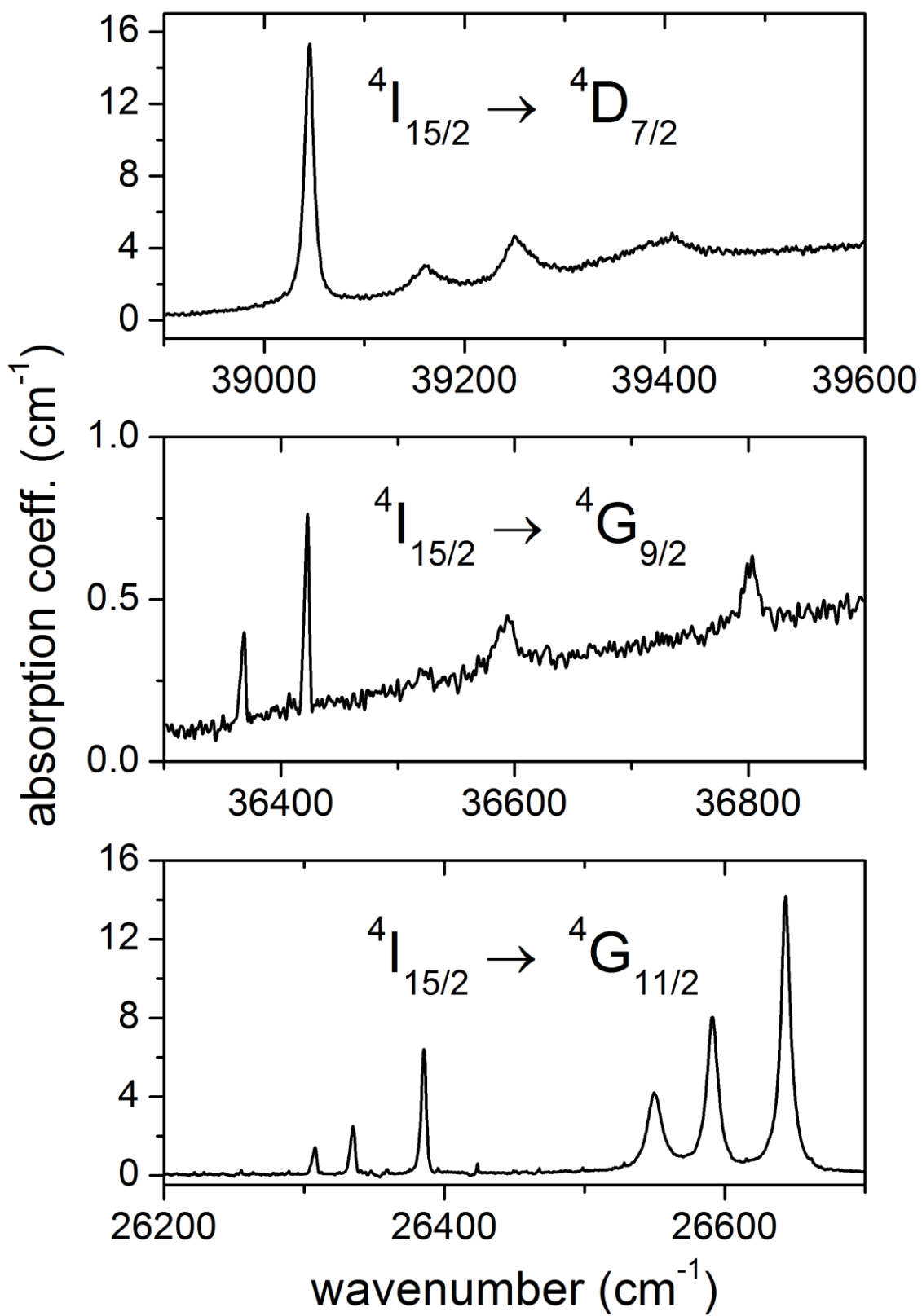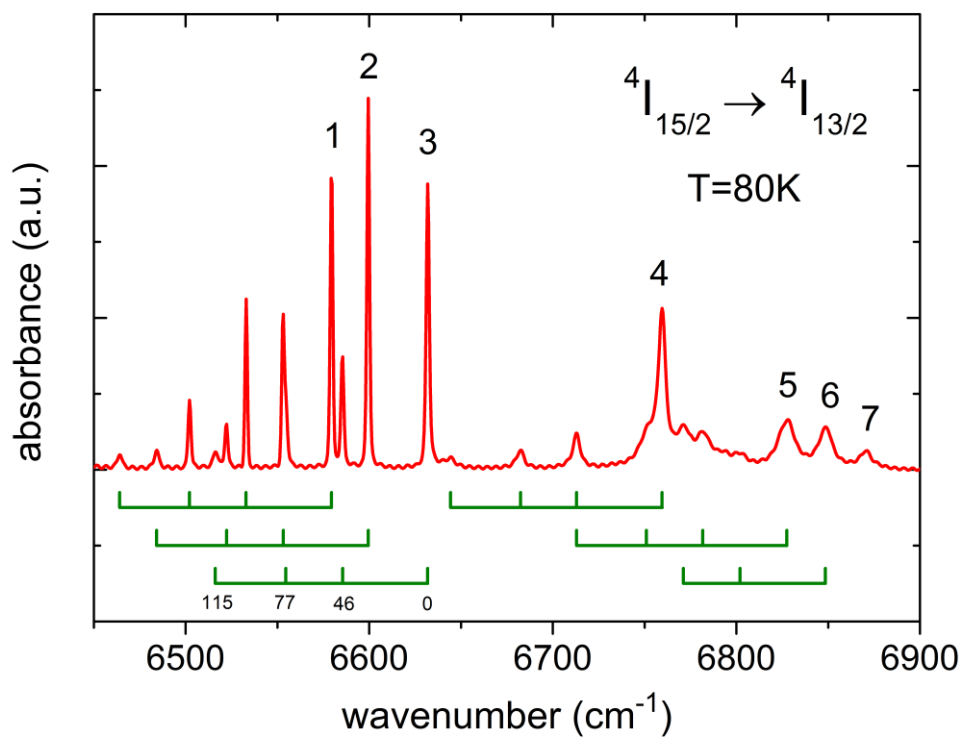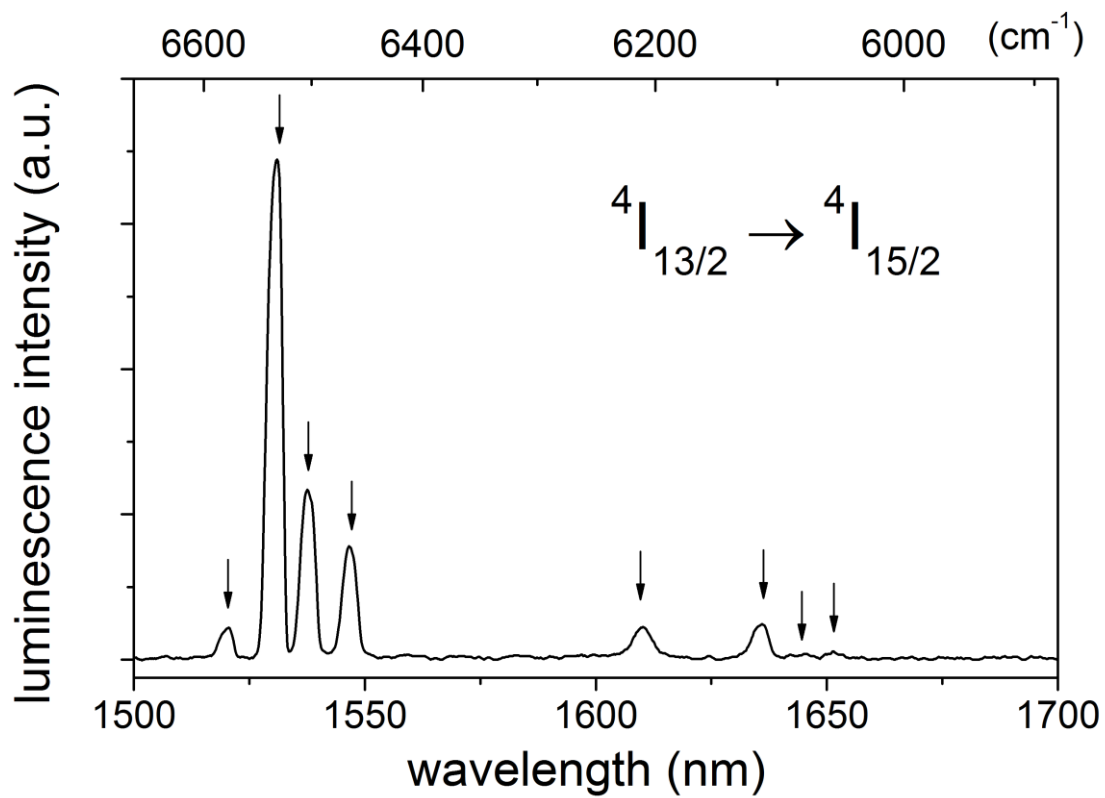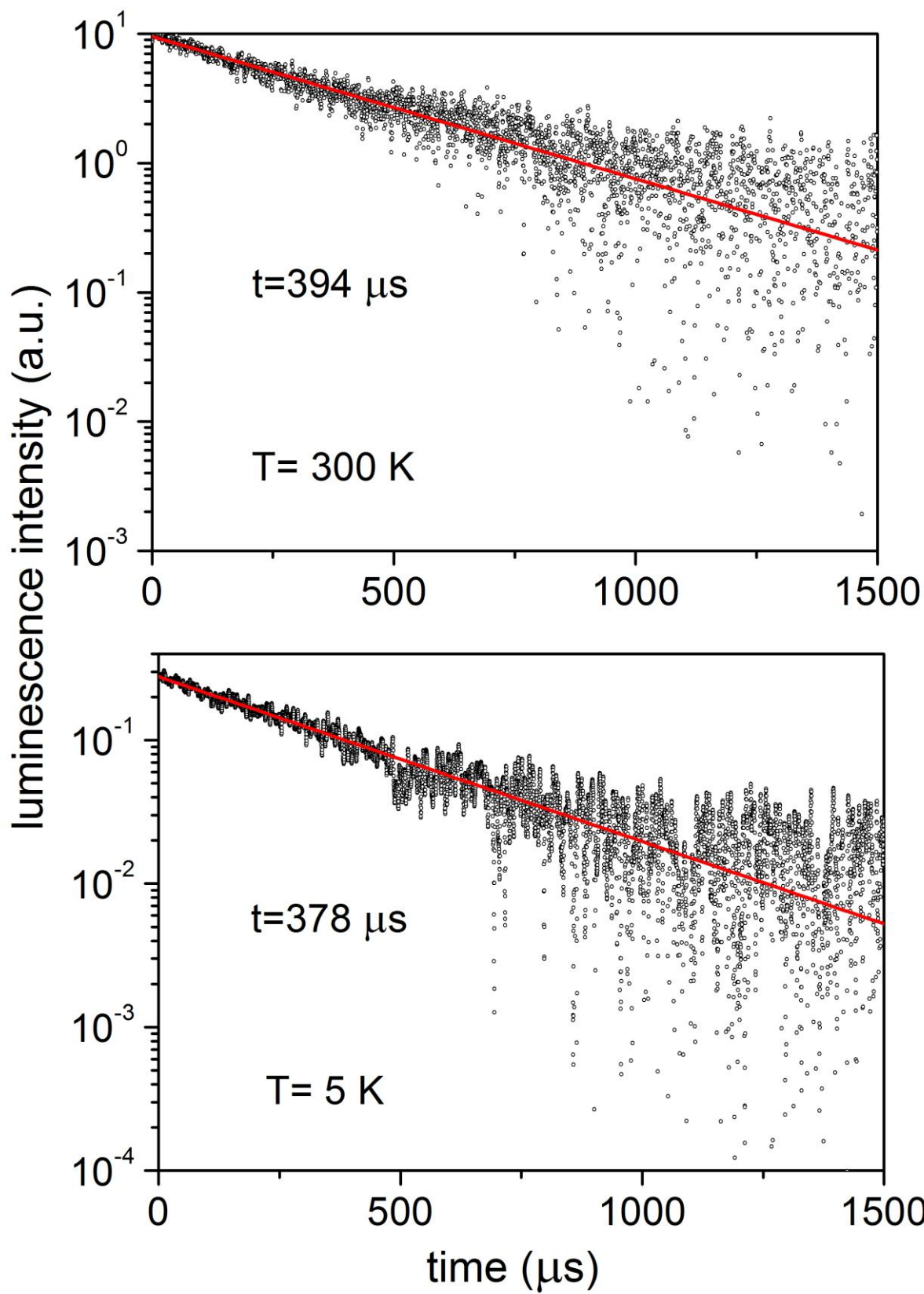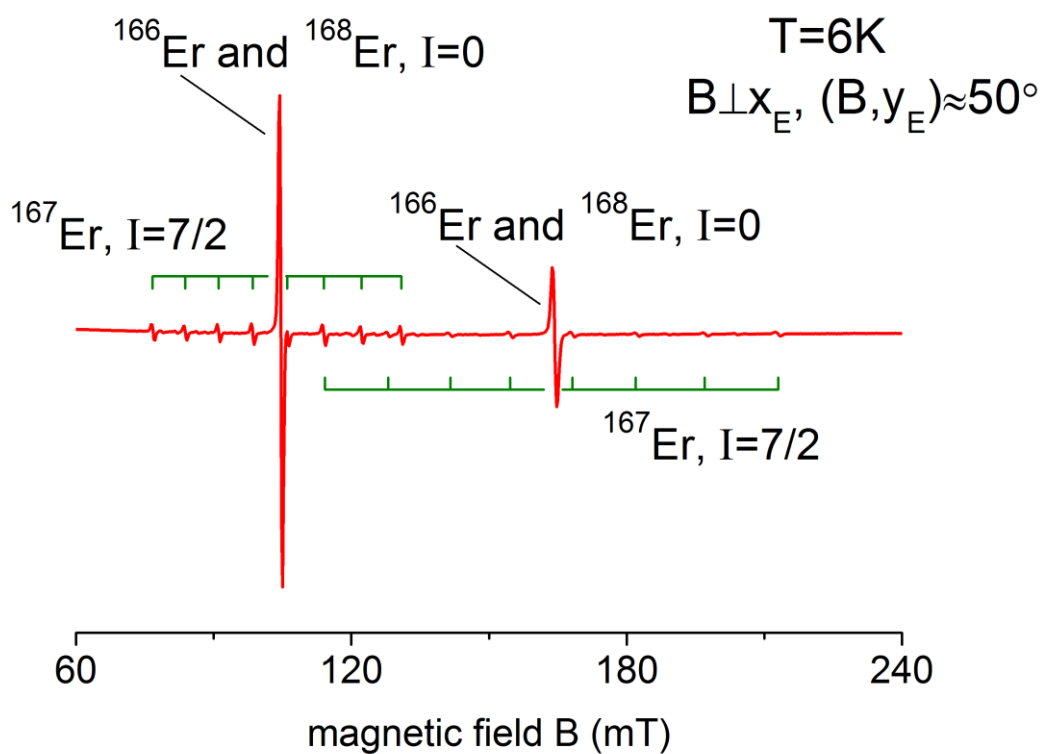
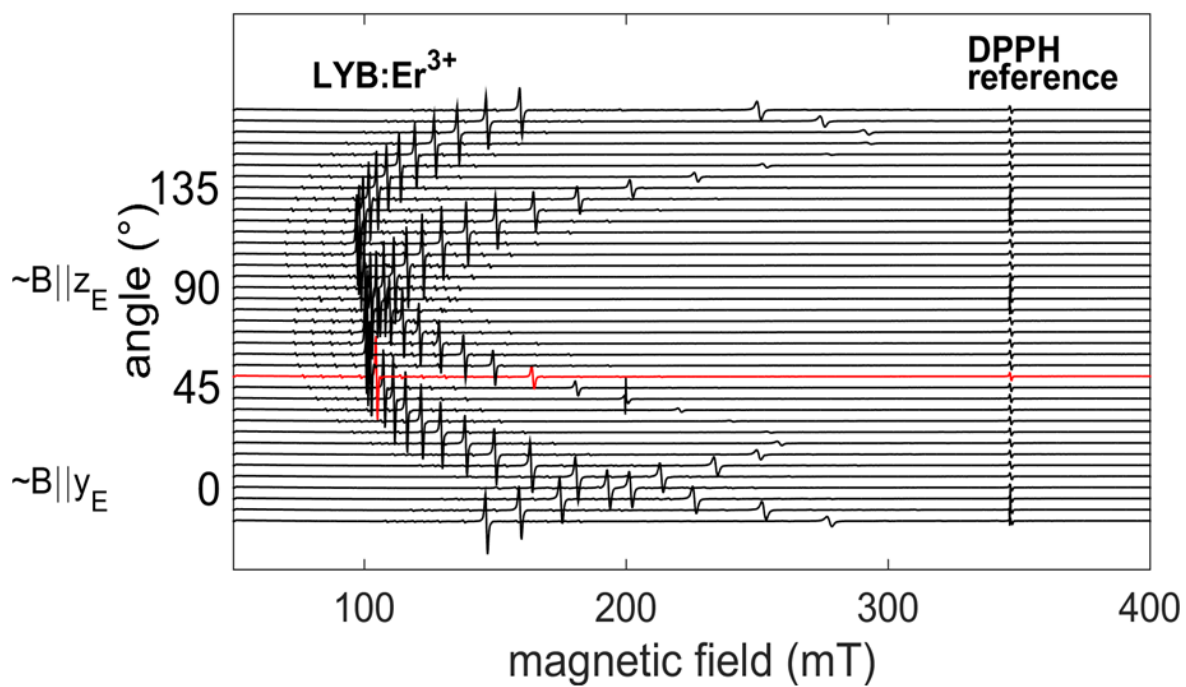Figure 1

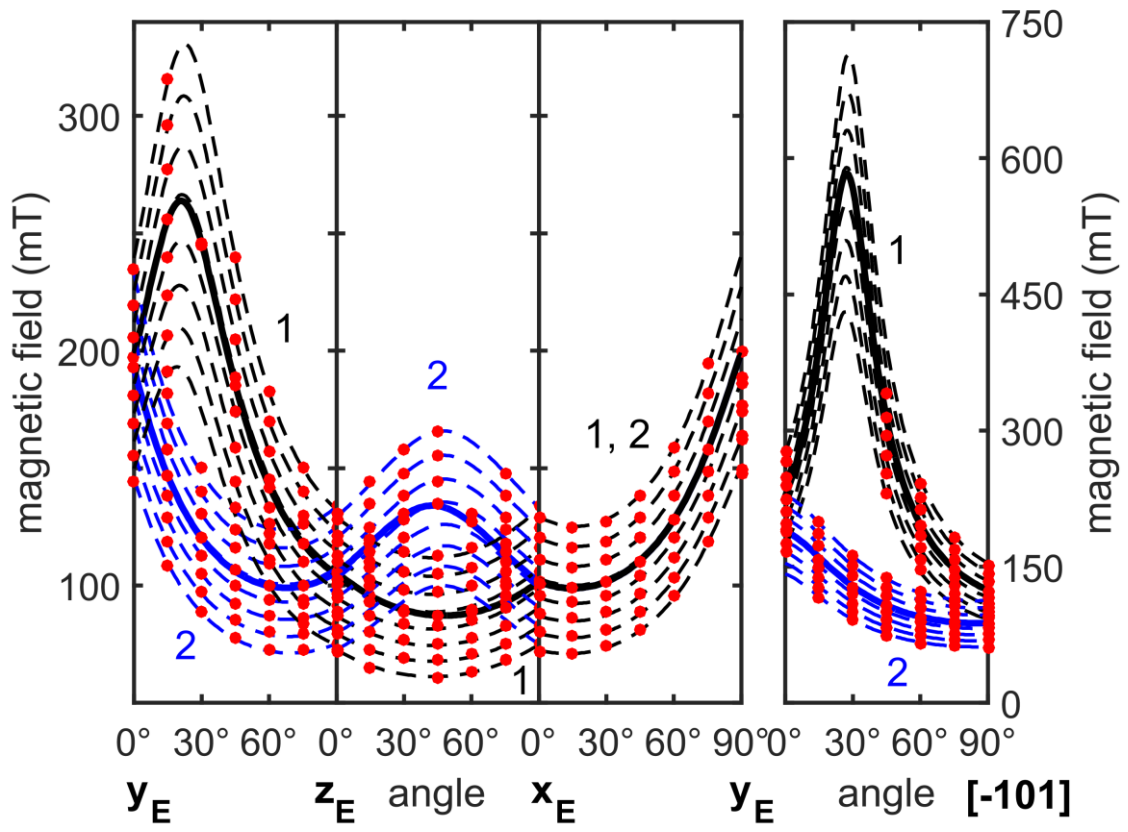Figure 2

Figure 3

Figure 4

Figure 5

Figure 6

Figure 7

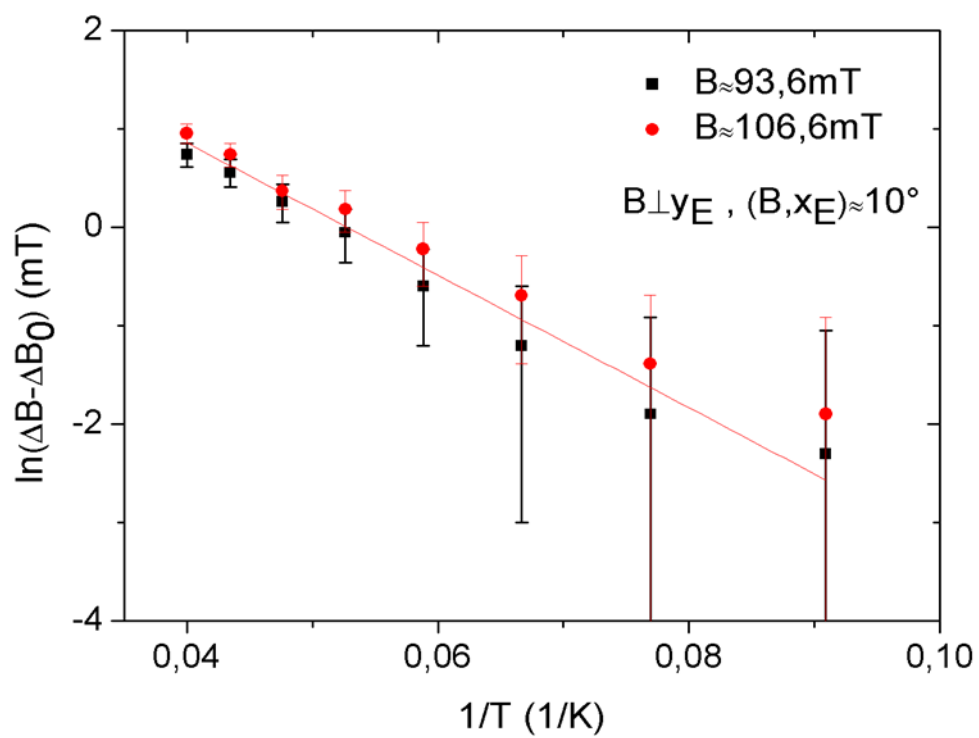Figure 8

References

[1]   T. Chao-Yuang, J. Ai-Dong, L. Zun-Du, *JIEGOU HUAXUE (J. Struct. Chem.)* **8** (1989) 215-219.

[2]   Z.D. Luo, H. Zhang, Y.D. Huang, M.W. Qiu, Y.C. Huang, C.Y. Tu, A.D. Jiang, *Crystal Research and Technology* **26** (1991) K5-K8.

[3]   J. Sablayrolles, V. Jubera, J.-P. Chaminade, I. Manek-Hönninger, S. Murugan, T. Cardinal, R. Olazcuaga, A. Garcia, F. Salin, *Optical Materials* **27** (2005) 1681-1685.

[4]   Y.W. Zhao, Y.F. Lin, Y.J. Chen, X.H. Gong, Z.D. Luo, Y.D. Huang, *Applied Physics B* **90** (2008) 461-464.

[5]   J. Sablayrolles, V. Jubera, M. Delaigue, I. Manek-Hönninger, J.-P. Chaminade, J. Hejtmanek, R. Decourt, A. Garcia, *Materials Chemistry and Physics* **115** (2009) 512-515.

[6]   G. Mandula, Z. Kis, K. Lengyel, É. Tichy-Rács, L. Kovács, I. Hajdara, *Applied Physics B*, to be submitted

[7]   C.W.E. van Eijk, *Radiation Measurements* **38** (2004) 337-342.

[8]   F. Zhang, Y. Wang, Y. Tao, *Journal of Luminescence* **136** (2013) 51-56.

[9]   J. Sablayrolles, V. Jubera, F. Guillen, R. Decourt, M. Couzi, J.-P. Chaminade, A. Garcia, *Optics Communication* **280** (2007) 103-109.

[10]   V. Jubera, M. Chavoutier, A. Artemenko, P. Veber, M. Velazquez, A. Garcia, *ChemPhysChem* **12** (2011) 1288-1293.

[11]   A. Brenier, A. Yoshikawa, K. Lebbou, A. Jouini, O. Aloui-Lebbou, G. Boulon, T. Fukuda, *Journal of Luminescence* **126** (2007) 547-550.

[12]   Yuwei Zhao, Xinghong Gong, Yanfu Lin, Zundu Luo, Yidong Huang, *Materials Letters* **60** (2006) 418-421.

[13]   Y.W. Zhao, X.H. Gong, Y.J. Chen, L.X. Huang, Y.F. Lin, G. Zhang, Q.G. Tan, Z.D. Luo, Y.D. Huang, *Applied Physics B* **88** (2007) 51-55.

[14]   A.P. Skvortsov, N.K. Poletaev, K. Polgár, Á. Péter, *Technical Physics Letters*, **39** (2013) 424-426.

[15]   Á. Péter, K. Polgár, M. Tóth, *Journal of Crystal Growth* **346** (2012) 69-74.

[16]   G.H. Dieke, *Spectra and Energy Levels of Rare Earth Ions in Crystals*, Interscience Publishers, New York (1968)

[17]   J.B. Gruber, J.R. Quagliano, M.F. Ried, F.S. Richardson, M.E. Hills, M.D. Seltzer, S.B. Stevens, C.A. Morrison, T.H. Allik, *Phys. Rev. B* **48** (1993) 15561-15573.

[18] G.W. Burdick, J.B. Gruber, K.L. Nash, S. Chandra, D.K. Sardar, *Spectroscopy Letters* **42** (2010) 406-422.

[19] J.R. Quagliano, N.I. Cockroft, K.E. Gunde, F.S. Richardson, *J. Chem. Phys*. **105** (1996) 9812-9822.

[20] W.T. Carnall, P.R. Fields, R. Sarup, *J. Chem. Phys*. **57** (1972) 43-51.

[21] I. Földvári, E. Beregi, A. Munoz F., R. Sosa, V. Horváth, *Optical Materials* **19** (2002) 241-244.

[22] S. Stoll, A. Schweiger, *Journal of Magnetic Resonance* **178** (2006) 42-55.

[23] D.S. Schonland, *Proc. Phys. Soc. London* **73** (1959) 788-792.

[24] H. Vrielinck, H.De Cooman, M.A. Tarpan, E. Sagstuen, M. Waroquier, F. Callens, *Journal of Magnetic Resonance* **195** (2008) 196-205.